Rare Metal Materials and Engineering
Volume 47, Issue 7, July 2018
Online English edition of the Chinese language journal

Available online at www.sciencedirect.com
ScienceDirect

Cite this article as: Rare Metal Materials and Engineering, 2018, 47(7): 1999-2004.

ARTICLE

Effect of Ag Content and β-PbO_2 Plating on the Properties of Al/Pb-Ag Alloy

Zhou Xiangyang [1], Wang Shuai[1], Ma Chiyuan[1], Long Bo[1], Wang Hui[1], Yang Juan[1], Guo Zhongcheng[2], Chen Buming[2]

[1] Central South University, Changsha 410083, China; [2] Kunming University of Science and Technology, Kunming 650093, China

Abstract: Due to the excellent electrical conductivity and mechanical properties, Al/Pb-Ag alloy has a great potential to be used as an alternative anode for zinc electrowinning. In this work, the effects of Ag content and surface plating with β-PbO_2 on the anodic behavior and reaction kinetics were investigated by cyclic voltammetry (CV), anodic polarization curves, electrochemical impedance spectroscopy (EIS) and corrosion rate test. The phase composition and microscopic morphology of the anode oxide layers after electrolysis were observed by X-ray diffraction (XRD) and scanning electron microscopy (SEM), respectively. The results indicate that high content of silver and electroplating β-PbO_2 layer can increase the oxygen evolution activity, electrocatalytic activity and corrosion resistance of the anodes. Al/Pb-0.75%Ag plating β-PbO_2 has the lowest oxygen evolution overpotential followed by Al/Pb-0.3%Ag plating β-PbO_2, Al/Pb-0.75%Ag and Al/Pb-0.3%Ag. Besides, high content of silver is more beneficial to improving corrosion resistance compared with electroplating β-PbO_2 on anode. In addition, the phase composition of four anodes layer are mainly composed of α-PbO_2, β-PbO_2, Pb and PbO.

Key words: Al/Pb-Ag alloy; plating β-PbO_2; oxygen evolution activity; zinc electrowinning

In the zinc electrowinning industry, the Pb-Ag (0.5%~1.0%) alloy is widely used due to its good corrosion resistance and stabilization in acidic sulfate solutions.[1-3] However, there are two main shortcomings which restrict its application. One is the high oxygen evolution overpotential (OEOP) resulting in high cell voltage and low cell efficiency. On the other hand, although high content of silver can enhance the mechanical properties of the anode, it undoubtedly increases the anode manufacturing costs. To tackle these problems, various alternative alloys are proposed to obtain a balance between anode performance and cost, that is, reducing the OEOP and the corrosion rate while keeping low manufacturing cost[4].

Studies have demonstrated that Pb-Ag-Ca alloy enhanced mechanical strength, and decreased the manufacturing cost by lowering the consumption of Ag. D. A. Rand et al[5] reported that a high Ca content could increase the corrosion rate because of the decreased grain size. J. Xu et al[6] found that the corrosion rate of the Pb-Sn alloy decreased with the increasing of Sn content; however, high Sn content of Pb-Sn alloy caused poor mechanical strength[7]. Compared with the cast Pb-Ag (1.0%) alloy, Pb-Co-Ti has good corrosion resistance, but does not reduce the oxygen evolution potential (OEP)[8]. The Pb-Ag-Sn-Co alloy significantly reduces the OEP and shows the least corrosion in comparison to Pb-Ag, Pb-Ag-Sr, Pb-Ag-Ba-As, Pb-Ag-Sn and Pb-Ag-As; however, the complex production process of these alloys restrict their wide spread commercial application[7,9]. Recently, Pb-based composite anodes and doping active particle have been widely studied[10-14], which could greatly improve the corrosion resistance and oxygen evolution activity of the anodes. Nevertheless, due to the weak adhesion between the active dispersed phase and lead substrate, these active deposited layers tend to crack or fall off when the composite anodes are applied in industry, thus severely affecting the service life of anodes.

Received date: July 25, 2017
Foundation item: National Nature Science Foundation of China (51304254 , 51274240); China Postdoctoral Science Foundation (2015M580698)
Corresponding author: Yang Juan, Ph. D., Associate Professor, School of Metallurgy and Environment, Central South University, Changsha 410083, P. R. China, Tel: 0086-731-88836329, E-mail: 646872865@qq.com

In recent years, Al/Pb-Ag alloy is proposed as a novel type anode, which not only maintains the alloy composition, but also does not need to coat active catalytic layer. Aluminum is employed as matrix due to its low cost and density, excellent mechanical properties and high conductivity. Owing to the application of aluminum substrate, the silver content is greatly reduced, mechanical performance of the anode is improved, and surface activity of the anode is comparable to that of the traditional Pb-Ag alloy. Besides, most of the literatures indicate that β-PbO_2 has excellent electrocatalytic activity and corrosion resistance, which could further improve the overall performance of anode[15,16]. Al/Pb-Ag anodes have been studied for several years, mostly in a relatively short time and at low current density[17,18]. However, only after a long time of electrolysis or high current density, the anode oxide film of Pb-Ag anodes can be in a stable state [19]. Therefore, the electrochemical properties of Al/Pb-Ag anode and Al/Pb-Ag plating β-PbO_2 anode with different Ag contents after 12 h galvanostatic electrolysis at a high current density of 10 000 $A \cdot m^{-2}$ were investigated to obtain the effect of Ag content and β-PbO_2 plating on the performance of anodes. The phase composition and microscopic morphology of the anode oxide after electrolysis were observed by XRD and SEM, respectively.

1 Experiment

The main raw materials are Al/Pb-0.3%Ag and Al/Pb-0.75%Ag alloy (Kunming Hendera Science and Technology Co. Ltd, China). Anode preparation processes were as follows: firstly, intercepting a piece of Al/Pb-Ag alloy; then degreasing, polishing, washing, airing and electroplating β-PbO_2; finally, Al/Pb-0.3%Ag, Al/Pb-0.75%Ag, Al/Pb-0.3%Ag plating β-PbO_2 and Al/Pb-0.75%Ag plating β-PbO_2 were connected to a plastic isolated copper wire and coated by epoxy resin and polyamide resin (2:1) with a working area of 1.0 cm×1.0 cm. For the convenient purpose, the experimental samples were numbered as shown in Table 1. After galvanostatic electrolysis for 12 h, the samples were studied by electrochemical test, XRD , SEM and corrosion rate test.

The composition and process conditions of the β-PbO_2 plating bath were as follows: MR electroplating bath, current density of 300 $A \cdot dm^{-2}$, bath temperature of 40 °C and electroplating for 3 h.

Table 1 Number and composition of the experimental sample

Samples	Anode type
1#	Al/Pb-0.3%Ag plating β-PbO_2
2#	Al/Pb-0.3%Ag
3#	Al/Pb-0.75%Ag plating β-PbO_2
4#	Al/Pb-0.75%Ag

Galvanostatic electrolysis of four anode samples was conducted at an anodic current density of 10000 $A \cdot m^{-2}$ in 150 $g \cdot L^{-1}$ H_2SO_4 at 35 °C. Then, the electrochemical measurements for the four anodes were carried out on an electrochemical workstation (PARSTAT2273, America) and performed in electrolyte of 50 $g \cdot L^{-1}$ Zn^{2+} and 150 $g \cdot L^{-1}$ H_2SO_4 at 35 °C using a single three-electrode system. The reference electrode and the counter electrode were saturated calomel electrode (SCE) and graphite electrode of 2 cm×5 cm, respectively. All potentials in this study were against SCE.

The scanning range of CV was -1.0~2.4 V with a sweep rate of 20 $mV \cdot s^{-1}$. Anodic polarization experiment was conducted at a constant scanning rate of 2 $mV \cdot s^{-1}$ from the initial potential of 1.7 V to the final potential of 2.1 V. The AC amplitude of EIS measurement was 10 mV root mean squared and the frequency range was from 10^5 Hz to 10^{-1} Hz, and the potential was 1.9 V.

In addition, the microscopic morphology and phase composition of the anodic oxide layers were observed using FEI-Quanta 200 scanning electron microscope and D/max-2200 X-ray diffractometer, respectively.

2 Results and Discussion

2.1 Cyclic voltammetry

The CV curves of four anodes are shown in Fig.1. The voltammetry curves are overall characterized by the two typical anodic peaks (a and c in Fig.1) at the positive scanning and by one cathodic peak (d in Fig.1) and one cathodic branch peak (e in Fig.1) during scanning in the negative direction[20].

The peak (a), (c) and (f) in Fig.1 of anode 3# is the highest, followed closely by that of anode 4#, 1# and 2#. For the peak (b), (d) and (e), the anode 3# is the highest, while anode 1#, 2# and 4# are almost the same.

According to some literatures[20,21], the peak (a) refers to the oxidation of Pb to $PbSO_4$, and the polarization area of 3# is the biggest compared with those for the other three anodes. It suggests that a larger number of $PbSO_4$ on the surface, which are the reaction site for the peak (c). In this potential field, small amounts of PbO, $PbO \cdot PbSO_4$ and $PbSO_4 \cdot H_2O$ may be also generated. The anodic peak (c) is ascribed to the oxidation of PbO to α-PbO_2, PbSO4 to β-PbO_2 and oxygen evolution reaction. The peak (c) shows that the four anodes have different oxygen evolution characteristics, and this depolarization is probably due to a variety of silver content and whether electroplating β-PbO_2 or not. There is a special peak (b) at 1.4~1.6 V during the scanning in the negative direction. This peak is due to the oxidation of Pb and SO_4^{2-} which diffuse into the anodic film. In other words, the peak (b) appears only in the presence of already formed PbO_2 at the positive scanning when the potential moves in the negative direction, which in turn contributes to the oxidation of Pb to $PbSO_4$.

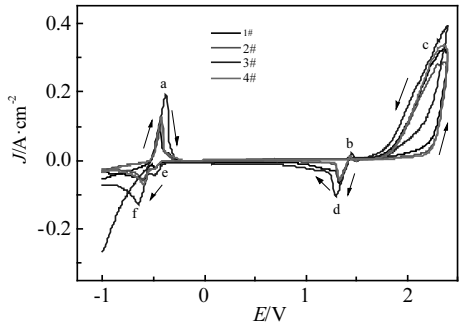

Fig.1 CV curves of four anodes

The cathodic peak (d) represents the reduction of α-PbO_2 and β-PbO_2 to $PbSO_4$. This peak is an indication of the α-PbO_2 and β-PbO_2 generated. The peak current density of 3# is 120 mA·cm^{-2}, while those of the other three anodes are about 70 mA·cm^{-2}. And this result is in agreement with the XRD results as illustrated below. Moreover, the reduction peak (c) shifts toward the negative direction corresponding to the shift of the oxidation peak (d). The cathodic peak (e) is due to the reduction of PbO and $PbSO_4$ to Pb. Furthermore, this peak of 3# is approximately twice as high as the other three anodes. Finally, the peak (f) corresponds to the reduction of $PbSO_4$ to Pb. Compared with the other three anodes, the peak of 3# is as high as twice and apparently moves about 120 mV toward the negative direction.

2.2 Anodic polarization and kinetic parameters for oxygen evolution

The OEOP (η) uses the following formula[13,19]:

$$\eta = E + 0.245\ \text{V} - 1.242\ \text{V} - iR_s \quad (1)$$

where E is the applied potential, 0.245 V is the potential of the SCE, 1.242 V is OEP in a synthetic zinc electrowinning electrolyte of 50 g·L^{-1} Zn^{2+}, 150 g·L^{-1} H_2SO_4 at 35 °C, and R_s is the electrolyte resistance between the working and reference electrodes, which can be obtained by the equivalent circuit parameters of EIS.

As shown in Fig.2, all fitting lines exhibit a double-slope behavior. According to the Tafel equation: $\eta = a + b\log i$. Where, η is OEOP, a is the Tafel constant, b is the Tafel slope, and i is electrode surface current density. Therefore, the curve of η(y-axis) and log$i$ (x-axis) is drawn, a and b can be acquired by the liner fitting for relationship curve of η and log$i$ in our study. Finally, the exchange current density of electrode surface, i_0, can be calculated by Tafel equation when η=0. The calculated kinetic parameters of oxygen evolution of four anodes are listed in Table 2.

In Table 2, the value of i_0 is extremely small and considered to be meaningless in evaluating the oxygen evolution activity of anodes. However, the value of OEOP, η, is relatively remarkable. Among the η of the four anodes, the order is as follows: 3#＜1#＜4#＜2#. As a result, both electroplating β-PbO_2 and high content of silver can improve oxygen evolution activity of the anode. Moreover, η of 1# is lower than that of 4#, indicating that electroplating β-PbO_2 can significantly enhance oxygen evolution activity of the anode compared to high content of silver. Table 2 shows that b_1 of 3# is the lowest compared with the other three anodes, but its b_2 is relatively larger. This is probably due to that the 3# anode presents a fine-grain anodic layer, large specific surface area and electrocatalytic effects of increased β-PbO_2 content[22], which can be further confirmed by Fig.5 as discussed below.

2.3 EIS characterizations

The reaction of oxygen evolution in acid solution is as follows: $2H_2O \rightarrow 4H^+ + O_2 + 4e^-$.

According to the relevant literature[23,24], the mechanism of oxygen evolution reaction consists of the following four steps:

$$S + H_2O \rightarrow S\text{-}OH_{ads} + H^+ + e^- \quad (2)$$

$$S\text{-}OH_{ads} \rightarrow S\text{-}O_{ads} + H^+ + e^- \quad (3)$$

$$2S\text{-}OH_{ads} \rightarrow S\text{-}O_{ads} + S + H_2O \quad (4)$$

$$S\text{-}O_{ads} \rightarrow S + 0.5O_2; \quad (5)$$

Where S is active sites on the oxide surface, and $S\text{-}OH_{ads}$, $S\text{-}O_{ads}$ are absorption intermediates. Step (3) and step (4) are usually supposed to be controlled by compact morphology and cracked morphology, respectively. Among the steps expressed above, the rate controlling step of a specific anode is determined by its Tafel slope. In general,

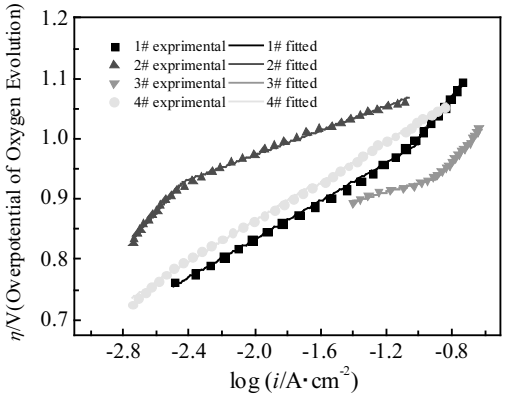

Fig.2 Tafel lines of four anodes

Table 2 Overpotential and kinetic parameters of oxygen evolution reaction of four anodes

Sample	b_1	b_2	η/V(i=0.05 A/cm^2)	i_0/A·cm^{-2}
1#	158.4	340.7	0.941	5.462×10^{-8}
2#	309.6	127.5	1.045	2.108×10^{-10}
3#	74.7	297.7	0.905	3.954×10^{-14}
4#	167.0	170.1	0.977	8.962×10^{-8}

step (2) is a rate controlling step, when the Tafel slope, b is $\geqslant$120 mV·dec^{-1}; if b is about 40 mV·dec^{-1}, step (3) and step (4) are rate controlling; and if b is approximate to 15 mV·dec^{-1}, step (5) is rate determining.

Table 2 shows that all the Tafel slopes of the four anodes are close to or larger than 120 mV·dec^{-1}, indicating that step (2) is regarded as a rate controlling step. It means that the reaction kinetic mechanism of four anodes is the same. Therefore, an equivalent electrical circuit (Fig.3)[25,26], using ZView 2.0 software, can be simulated by the oxygen evolution reaction. As shown in Fig.3, the experimental (spots) and simulated (lines) data can reach a good agreement. Where R_s is the solution resistance; C_{dl} represents the double-layer capacitance at the anode/electrolyte interphase; R_t is the charge transfer resistance of the anode reaction; R_a and C_a represent the equivalent resistance and capacitance connected with absorption of intermediate (S-OH$_{ads}$), respectively.

Table 3 shows that R_t plays an important role in the whole impedance. Besides, the R_t of 3# is the largest compared with the other three anodes, and the R_s and R_a are also comparatively large. This is due to its compact anodic film, which hinders the mass transfer of electrolyte, and leading to the increase of the charge transfer resistance and the solution resistance. The results correspond with Fig.4.

2.4 Microscopic surface morphology and phase composition

Fig.4 shows the microscopic surface morphologies of the four anodes.

1#, 2# and 4# present a severely corrosive microstructure and a high porosity amorphous film is clearly seen to extend to the whole anode surface. Besides, both 2# and 4# show many cavities and deep holes, indicating the worst corrosion resistance. This means that a high content of silver enhances the anode corrosion resistance. Nevertheless, 3# has changed dramatically, presents the most regular and compact structure among the four anodes, indicating the highest corrosion resistance in the electrolyte. In addition, the uniform granules of 3# indicates that the large specific surface area can result in a smaller effective current density and lower anodic potential in this electrolyte compared with other anodes.

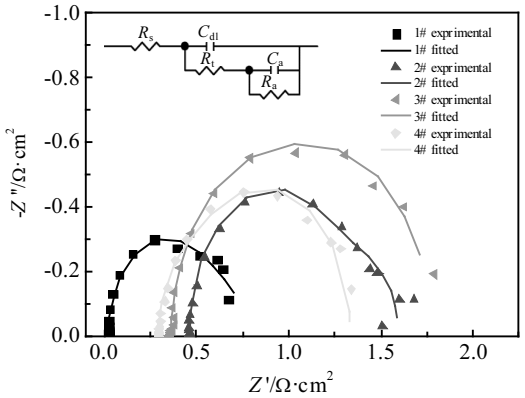

Fig.3 EIS spectra and electrical equivalent circuit of four anodes

Table 3 Equivalent circuit parameters of four anodes corresponding to the spectra in Fig.3

Anode	R_s/Ω·cm^2	C_{dl}/F·cm^{-2}	R_t/Ω·cm^2	C_a/F·cm^{-2}	R_a/Ω·cm^2
1#	0.0245	0.0408	0.6004	1.04	0.1255
2#	0.4645	0.0203	0.9039	0.618	0.2281
3#	0.3648	0.0594	1.093	0.4695	0.3134
4#	0.2984	0.0118	0.6354	0.0341	0.3997

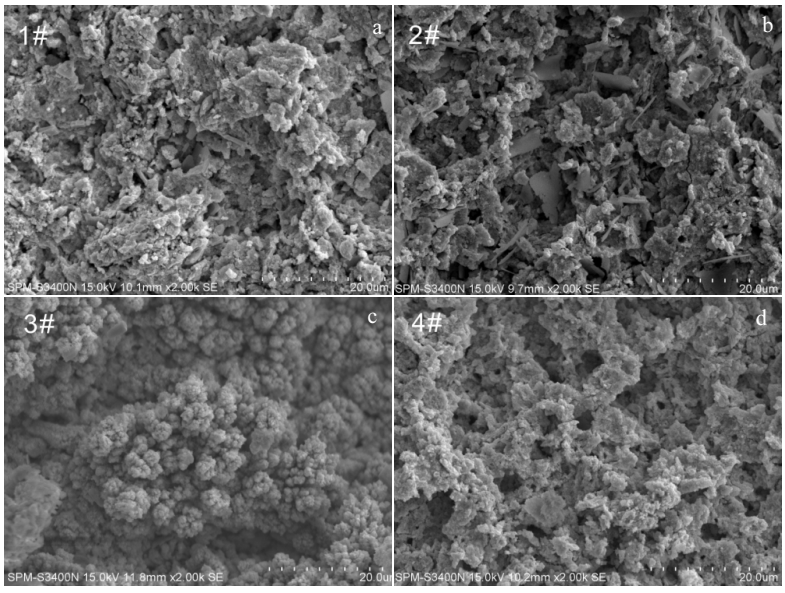

Fig.4 SEM images of surface morphologies of the four anodic oxide layers: (a) 1#, (b) 2#, (c) 3#, and (d) 4#

Fig.5 shows that the phase composition of four anodes are mainly composed of α-PbO_2, β-PbO_2, Pb and PbO. The major phase of oxide layer 1# and 2# consist of α-PbO_2 and PbO. While 2# presents low fraction of β-PbO_2, indicating that the electroplating β-PbO_2 film has fallen from the anode surface after electrolysis at high current density. Corresponding to Fig.5, the peak intensities of all the phase of 4# layer become average compared to the other three anodes. However, the major phase of 3# oxide layer is composed by α-PbO_2 and β-PbO_2 as well as a small amount of Pb and PbO. In fact, the peak intensity of β-PbO_2 of this layer is the highest among four anodes, and the peak intensity of α-PbO_2 is also relatively high. What is more, β-PbO_2 contributes to the oxygen evolution reaction due to its better electrocatalytic activity. Theoretically, 3# should have excellent oxygen evolution activity and low OEOP.

2.5 Corrosion rate

The corrosion rate of anode can be described with the formula:

$$V = \frac{m_0 - m_1}{St} \quad (6)$$

Where, V represents corrosion rate; m_0 and m_1 represent anode quality before and after electrolytic, respectively; S is effective area of anode surface, and its value is $4.396\times 10^{-4}m^2$; t represents electrolysis time.

According to Table 4, the corrosion rate of four anodes is as follows: 3#＜4#＜1#＜2#. It is well known that the corrosion rate is determined by electrolyte composition, current density and anode material. In this study, four different anode materials are adopted while keeping all other experimental conditions fixed. Therefore, the anode corrosion rate in our study is controlled by the composition of anodes. As shown in Table 4, the corrosion resistance of 3# is the best, while that of 2# is the worst. In addition, the corrosion resistance of 4# is lower than that of 1#, indicating that a high content of silver is more helpful to improve corrosion resistance compared with electroplating β-PbO_2 on anode.

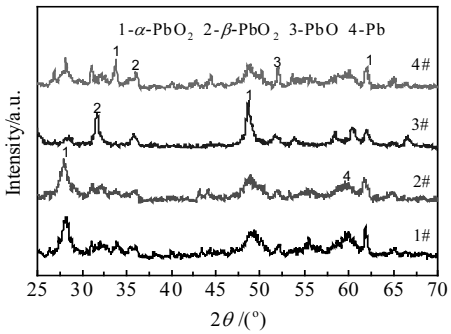

Fig.5 XRD patterns of four anodic surface

Table 4 Corrosion rate of four anodes after 12 h electrolysis

Anode	(m_0-m_1)/g	V/g·h^{-1}·m^{-2}
1#	0.132	25.023
2#	0.1485	28.151
3#	0.1087	20.606
4#	0.1224	23.203

3 Conclusions

1) Al/Pb-0.75%Ag plating β-PbO_2 has the lowest oxygen evolution overpotential followed by Al/Pb-0.3%Ag plating β-PbO_2 and Al/Pb-0.75%Ag and then Al/Pb-0.3%Ag. Moreover, electroplating β-PbO_2 significantly enhances oxygen evolution activity of the anode compared with a high content of silver.

2) The oxygen evolution reaction mechanism of four anodes is controlled by the generation and consumption of S-OH_{ads}, and the charge transfer resistance (R_t) takes a dominant part in the whole reaction resistance. Compared with the other three anodes, the R_t of Al/Pb-0.75%Ag plating β-PbO_2 is the largest due to its compact anodic layer.

3) Al/Pb-0.75%Ag plating β-PbO_2 presents the most regular, compact structure and excellent corrosion resistance, while the other three anodes perform relatively serious corrosive microstructure and complex crystal grains. The phase composition of four anodes are mainly composed of α-PbO_2, β-PbO_2, Pb and PbO. However, the proportions of these phases gradually vary by different anodes.

4) Al/Pb-0.75%Ag plating β-PbO_2 has the best corrosion resistance followed by Al/Pb-0.75%Ag and Al/Pb-0.3%Ag plating β-PbO_2 and then Al/Pb-0.3%Ag. Furthermore, a high content of silver is more contribute to improve corrosion resistance compared with electroplating β-PbO_2 on anode.

References

1 Felder A, Prengaman R D. *Journal of the Minerals, Metals & Materials Society*[J], 2006, 58(10): 28

2 Lafront A M, Zhang W, Ghali E *et al. Electrochimica Acta*[J], 2010, 55(22): 6665

3 Jaimes R, Miranda-Hernández M, Lartundo-Rojas L *et al. Hydrometallurgy*[J], 2015, 156: 53

4 Yu P, O'Keefe T J. *Journal of the Electrochemical Society*[J], 1999, 146(4): 1361

5 Rand D A J, Boden D P, Lakshmi C S *et al. Journal of Power Sources*[J], 2002, 107(2): 280

6 Xu J, Liu X B, Li X G *et al. Journal of Power Sources*[J], 2006, 155(2): 420

7 Ivanov I, Stefanov Y, Noncheva Z *et al. Hydrometallurgy*[J], 2000, 57(2): 109

8 Dobrev T, Valchanova I, Stefanov Y *et al. Transactions of The Institute of Metal Finishing*[J], 2013, 87(3): 136
9 Lai Y Q, Jiang L X, Li J *et al. Hydrometallurgy*[J], 2010, 102(1-4): 73
10 Schmachtel S, Toiminen M, Kontturi K *et al. Journal of Applied Electrochemistry*[J], 2009, 39: 1835
11 Mohammadi M, Alfantazi A. *Hydrometallurgy*[J], 2016, 159: 28
12 Ma R X, Cheng S Y, Zhang X Y *et al. Hydrometallurgy*[J], 2016, 159: 6
13 Xu R D, Huang L P, Zhou J F *et al. Hydrometallurgy*[J], 2012, 125-126: 8
14 Yang H T, Chen B M, Liu H R *et al. International Journal of Hydrogen Energy*[J], 2014, 39(7): 3087
15 Zhao J, Zhu C Z, Lu J *et al. Electrochimica Acta*[J], 2014, 118: 169
16 Zhu C Z, Hu C J, Lu J *et al. Russian Journal of Electrochemistry*[J], 2015, 51(4): 353
17 Zhang Y C, Chen B M, Yang H T *et al. Transactions of Nonferrous Metals Society of China*[J], 2014, 24(3): 893
18 Zhang Y C, Chen B M, Yang H T *et al. Journal of Central South University*[J], 2014, 21(1): 83
19 Yang H T, Liu H R, Guo Z C *et al. Hydrometallurgy*[J], 2013, 140: 144
20 Clancy M, Bettles C, Stuart A *et al. Hydrometallurgy*[J], 2013, 131-132: 144
21 Rashkov St, Stefanov Y, Noncheva Z *et al. Hydrometallurgy*[J], 1996, 40(3): 319
22 Li Y, Jiang L X, Lv X J *et al. Hydrometallurgy*[J], 2011, 109(3-4): 252
23 Prachi S, Michael S M. *Journal of Applied Electrochemistry*[J], 2009, 39(1): 107
24 Aromaa J, Forsen O. *Electrochimica Acta*[J], 2006, 51(27): 6104
25 Lai Y Q, Li Y, Jiang L X *et al. Hydrometallurgy*[J], 2012, 115-116: 64
26 Lai Y Q, Li Y, Jiang L X *et al*. *Journal of Electroanalytical Chemistry*[J], 2012, 671: 16

银含量和 β-PbO_2 镀层对 Al/Pb-Ag 合金性能的影响

周向阳[1]，王　帅[1]，马驰原[1]，龙　波[1]，王　辉[1]，杨　娟[1]，郭忠诚[2]，陈步明[2]

(1. 中南大学, 湖南 长沙 410083)

(2. 昆明理工大学, 云南 昆明 650093)

摘　要：采用循环伏安曲线(CV)、阳极极化曲线、电化学阻抗曲线(EIS)和腐蚀速率测试研究了不同银含量和镀层的 Al/Pb-Ag 阳极的阳极行为和反应动力学；用 X 射线衍射仪和扫描电镜观察了阳极氧化膜层的组分和表面形貌。结果表明，电镀 β-PbO_2 和高含量的银都能提高阳极的析氧活性、电催化活性以及耐腐蚀性。 Al/Pb-0.75%Ag 镀 β-PbO_2 具有最低的析氧过电位，其次是 Al/Pb-0.3%Ag 镀 β-PbO_2，再其次是 Al/Pb-0.75%Ag，最后是 Al/Pb-0.3%Ag。然而，与镀 β-PbO_2 相比，高含量的银更能有助于提高阳极的耐腐蚀性。此外，4 种阳极层的物相是 α-PbO_2、β-PbO_2、Pb 和 PbO。

关键词：Al/Pb-Ag合金; 镀β-PbO_2; 析氧活性; 电积锌

作者简介：周向阳，男，1969 年生，博士，教授，中南大学冶金与环境学院，湖南 长沙 410083, 电话: 0731-88836329, E-mail: xyzhou@csu.edu.cn